Int. J. Electrochem. Sci., 8 **(2013)** 9644 - 9651

International Journal of
ELECTROCHEMICAL
SCIENCE
www.electrochemsci.org

Electrochemical Characterization of Cellular Si and Si/C Anodes for Lithium Ion Battery

Tao Jiang[1], *Shichao Zhang*[2,*], *Ruoxu Lin*[2], *Guanrao Liu*[2], *Wenbo Liu*[2]

[1] Patent Examination Cooperation Center of the Patent Office,SIPO,Beijing 100191,China
[2] School of Materials Science and Engineering, Beijing University of Aeronautics and Astronautics, Beijing 100191, China
[*]E-mail: csc@buaa.edu.cn

Received: 13 May 2013 / *Accepted:* 29 May 2013 / *Published:* 1 July 2013

The structural optimization of Si-based anodes for lithium ion battery is always a promising way to put them into commercial application. In this article, cellular silicon-based anodes were prepared by casting milled Si and Si-C powders into the "valley-ridge" copper architecture. Their electrochemical properties and failure mechanism were studied by means of charge-discharge (C-D) test, differential capacity plots and electrochemical impedance spectroscopy (EIS). In comparison with common anode fabricated with "slurry-coating" technology on flat copper foil, the cellular copper framework has shown a great structural advantage in restricting severe volume changes of silicon particles. This "stress-restriction" environment can effectively suppress stain-induced loosening happened inside electrodes, and consequently improve cycle-life and coulombic efficiency of Si-based anodes.

Keywords: lithium ion battery; anode; current collector; silicon

1. INTRODUCTION

To meet the demand of modern portable electronic devices, active materials with high energy for lithium ion batteries have attracted much attention in recent years[1-3]. Among various types of anode materials, the silicon is an attractive candidate with its high theoretical specific capacity of nearly 4200 mAh g^{-1} in a fully lithiated state ($Li_{22}Si_5$) [4-7]. However, the dramatic capacity fading prevents its commercial application. Volume variation, over 300 %, is responsible for this problem. Many efforts have been made to overcome this problem, including introducing a secondary material such as graphite. As carbonaceous matrix, the graphite assumes multiple roles. First, it can significantly enhance electrical conductivity of the electrode. Moreover, it plays a positive role of "buffer" that can reduce mechanical strain stemming from the volume changes and hence impede

failure of the electrodes [8-12]. Simultaneously, some three-dimensional (3D) substrates, such as carbon paper, nickel foam *et al* [13-15], have been used as current collectors for lithium ion battery. The 3D structure can offer a good conductive and stress-restriction environment, leading to better electrochemical performance of anode. Recently, we have fabricated a novel cellular copper architecture through multiplestep electrodeposition and successfully used it in tin-based composite anode [16].

In this article, A silicon-based cellular anode was prepared by casting milled Si and Si/C powders into the cellular copper architecture. Their electrochemical properties and failure mechanism are respectively presented and discussed in details.

2. EXPERIMENTAL

The discharging-charging cycling tests were performed using two electrode coin cells. Silicon powders (Beijing Chemical Reagent, 300 mesh) were firstly milled for 8 h at 300 rpm using high-energy mechanical milling in Ar. Pure Si electrodes were prepared by casting slurries of 72 wt % Si, 20 wt % carbon black and 8 wt % polyvinylidene fluoride (PVDF) dissolved in N-methylpyrrolidinone (NMP) onto 3D copper current collector and flat copper foil. Subsequently, Graphite (TIMICAL, Switzerland) and milled silicon were mixed by weight ratio of 7:3 for the second 1 h milling. Si/C electrodes contain different proportions of 77 % active materials, 15 % carbon black and 8 % PVDF. All electrodes were dried and compressed under pressure of 10 MPa. The area density of active materials is kept similar to about 3.6-4.1 mg cm^{-2}. Test cells were assembled with electrodes (0.8 cm×0.8 cm), lithium foil and polypropylene separators in an Ar filled glovebox. A 1.0 M $LiPF_6$ solution in a 1:1 (volume ratio) mixture of ethylene carbonate (EC) and diethyl carbonate (DEC) was used as the electrolyte. A C-D cycle consisted of two steps: (*i*) discharging (lithiating) at a constant current of 0.2 mA mg^{-1} until either the selected specific capacity or the zero potential was reached; (*ii*) charging (delithiating) at 0.2 mA mg^{-1} until cutoff potential of 1.5 V.

AC electrochemical impedance spectroscopy (EIS) analysis was performed on PARStat 2273 using a sealed three-electrode cell with two lithium foils as both counter and reference electrodes. After the electrodes were charged at 0.01 mA mg^{-1} up to 1.5 V vs Li/Li^+, and left on open circuit for 2 h to obtain equilibrium, EIS measurements were carried out over the frequency ranging from 60 kHz to 10 mHz with ac amplitude of 5 mV. The morphology of electrodes was observed with the aid of scanning electron microscope (SEM, KYKY-2800).

3. RESULTS AND DISCUSSION

Fig.1a and b show the top and cross-section SEM micrographs of cellular copper substrate. The structure is made up of “valleys” with a wide pore size distribution of 20 μm ~90 μm and “ridges” constructed of deposited copper particles. Aside from suitable morphology, the cellular copper substrate also has excellent mechanical property. Mechanical test has demonstrated that its

compressive resistance is up to 4.8MPa. The satisfying strength, together with a coarse surface (Fig.1a) obtained by virtue of special control during the electrodeposition, guarantees better contact between Si-based powders and the substrate. Fig.1c shows the SEM image of pure Si cellular anode. The active materials have been separated by interconnected copper walls, forming a cell-like structure. Si/C anodes with similar configuration have not been shown here.

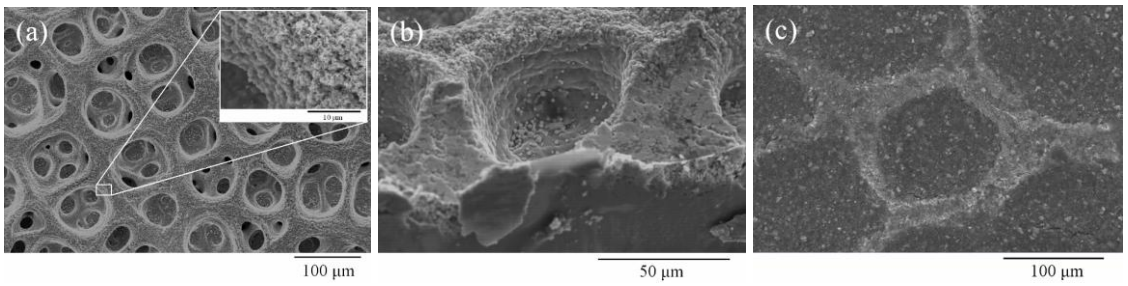

Figure 1. SEM micrographs of (a, b) cellular copper substrate prepared by multiplestep electrodeposition and (c) cellular Si anode.

Fig.2 shows the results of a comparative cycling test for electrodes prepared with copper foil and 3D architecture. In the case of pure Si anodes, the selected discharge capacity is 1200mAh/g in the initial cycle and 800mAh/g during the following cycles. Common 2D electordes have finished only 39 cycles, and their coulombic efficiency steps down to 90% □□after 26 cycles, resulting from increasing irreversible capacity.

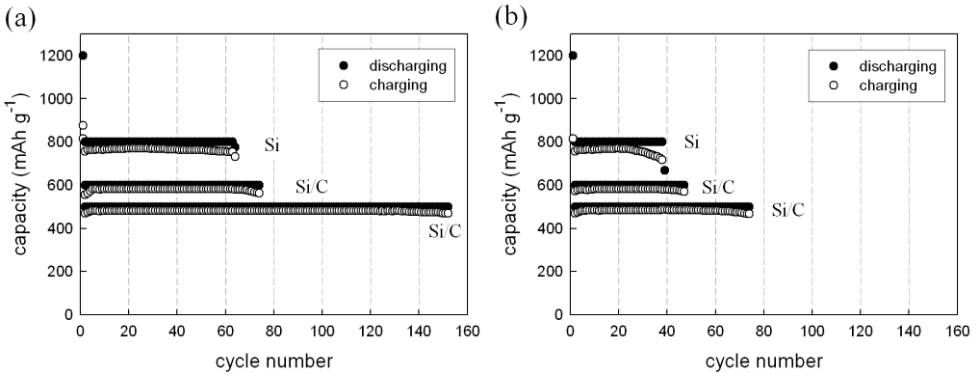

Figure 2. Cycle performance of (a) cellular and (b) common two-dimensional pure Si and Si/C anodes with a selected discharge capacity.

By contrast, the cellular electrodes show a better performance with a completion of 63 cycles until the discharge capacity can not reach 800mAh/g. More importantly, they keep a high coulombic efficiency above 90% □□even after the last cycle. Similar results are obtained in the test of Si/C electrodes. With the aid of cellular substrate, the cycling performance has been respectively improved to 73 and 152 cycles under two discharging conditions, which shows more advantages than 2D electrodes. Besides, when the selected capacity is 500mAh/g, the Li-storage capacity of Si is about

799mAh/g, corresponding to 800mAh/g of anterior pure Si electordes, if regarding the Li-storage capacity of graphite as theoretically 372mAh/g. Meanwhile, the cycling life of both electrodes has been greatly prolonged as shown in Fig.2. This improvement should be mainly attributed to the amelioration of conductivity environment and so-called "buffer" action coming from the introduction of graphite[8-12].

In order to further investigate the electrochemical behavior of these Si-based electrodes in discharging/charging process, the differential capacity plots were recorded and shown in Fig.3. During the first Li insertion, crystal silicon will experience an electrochemically-driven amorphization process. However, this process depends on many factors, such as transport rate of Li^+ into bulk silicon, the rate of amorphous Si-Li phase formation and the discharging/charging ways [17-20]. As shown in Fig.3a and Fig. 3c, a gradual "activation" phenomenon can be found at the beginning of test. A cathodic peak located at about 0.22 V emerges from the 2nd cycle and evolves in subsequent cycles. In the case of cellular Si anodes, two extraction peaks located at 0.35V and 0.50V appear in the first cycle. With the increase in test number, peak at 0.50V becomes higher gradually, which means that the Li extraction at high potential accounts for rather large proportion among total charging capacity. The situation seems a little different after the 25th cycle. Area of the peak at 0.50V has faded off with cycles, while the other one at 0.35V increases and its location shifts slightly to a lower potential. Similar evolvement of extraction peaks happens in the cycling test of 2D Si anodes. However, peak at high potential decreases as early as the 9th cycle and disappears in the 18th cycle. The performance indicates that the structural integrity of 2D electrode has been rapidly destroyed by enormous volume changes during charging/discharging. The differential capacity plots of cellular Si/C electrodes have been shown in Fig.3e and f. There is a striking difference in the first discharging curve: a broad dimple can be observed between 0.3V and 0.8V, but it has disappeared in the 2nd cycle. This reduction current should be attributed to the formation of a solid electrolyte interphase (SEI) film on graphite. Due to the Li extraction from graphite, a plateau can be found on the left of the first anodic peak at 0.35V in initial several cycles. With the activation of silicon, the plateau disappears and Si undertakes most of discharging capacity, which means that actual capacity contribution from Si is probably much higher than calculated results. This cycling way is actually unfavorable because excess burden of Si will accelerate the electrode failure. When more and more Si powders lose their electrochemical activities, the graphite will act as the main Li-storage material again. That is why Li-C extraction peak recurs in the last several cycles as shown in Fig.3f.

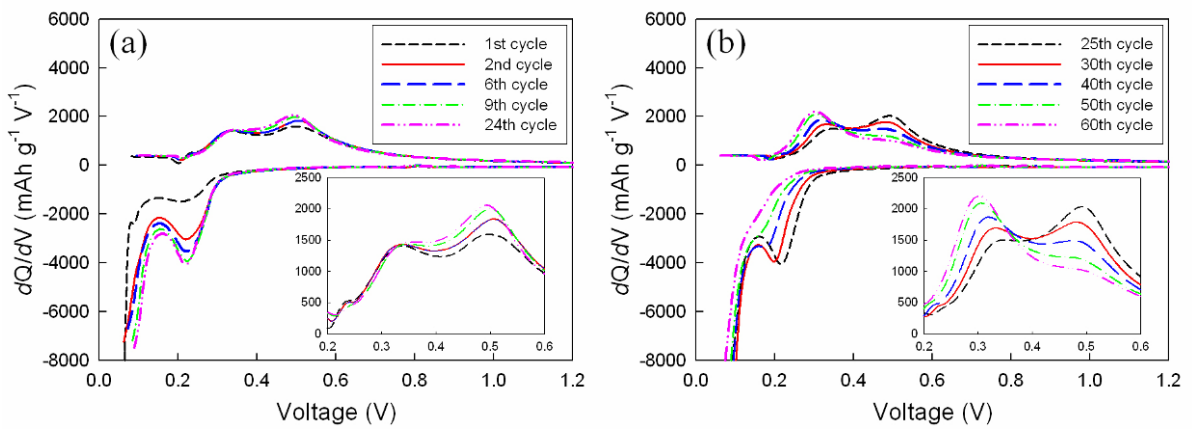

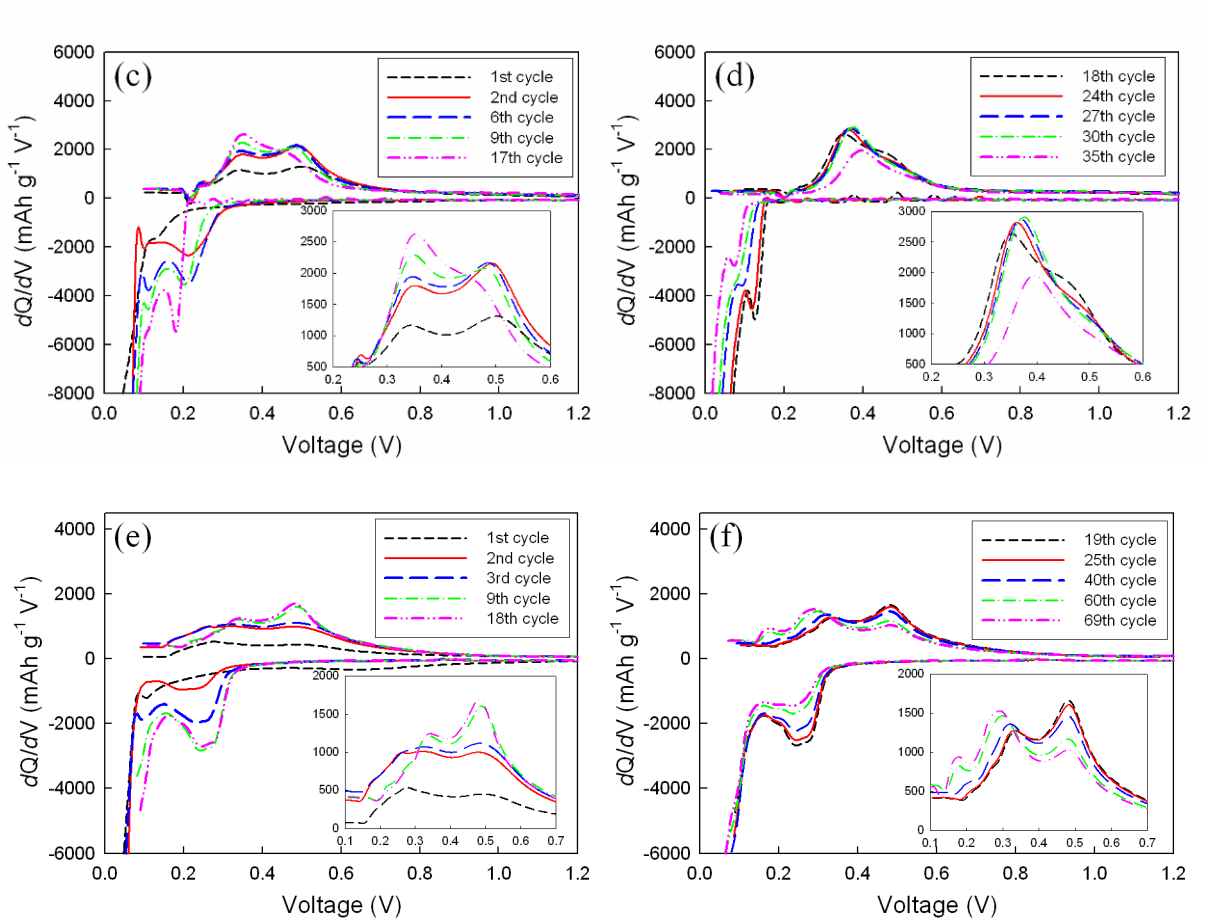

Figure 3. Differential capacity plots of different Si-based anodes: (a, b) cellular pure Si anodes with a selected discharge capacity of 800mAh/g; (c, d) two-dimensional pure Si anodes with a selected discharge capacity of 800mAh/g and (e, f) cellular Si/C composite anodes with a selected discharge capacity of 600 mAh/g.

Si particles will experience a durative contraction during de-alloying. Especially after 0.35V, they will contract in volume more drastically. Part of them begins to lose electric contact with the conductive additives and current collector, which ultimately results in increased resistance in electrodes [21-23]. From this point of view, it can be concluded that the rapid attenuation of extraction peak at high potential is a result of deteriorated conductivity environment. In comparison, the decelerated fading of extraction peak indicates that the cellular substrates play a positive role in relieving strain-induced failure. To support this point, EIS measurements were conducted after the electrodes were charged up to 1.5V vs. Li/Li^+ at 0.01mA mg^{-1}. It has been reported that the diameter of semicircle in high frequency region is mainly induced from the intrinsic electronic resistance and contact resistance of the electrode after the electrode is fully charged [24-26]. Fig.4 shows the variation of electrode resistance as function of cycling. Because of Li^+ trapping and formation of Si-Li alloy with high electronic conductivity, the internal resistance in both electrodes decreases in initial cycles. However, the resistance in 2D electrode increases rapidly to 238Ω after 20^{th} cycle, which is obviously higher than 81.1Ω in cellular electrode. In fact, the improved performance of cellular anodes should be mainly attributed to the "stress-restriction" environment in 3D metallic architecture. Si particles will

swell with the insertion of Li^+, but the severe volume changes can be restricted into a cell scale. The stress distributes homogeneously on metallic framework, and the generated resilience will promote a contraction of the whole materials, not only Si particles, during the Li extraction and suppress loosening inside the electrode. In addition, the resultant force for an integrate cell keeps balance by dispersing internal stress to around wall of micropores and simultaneously receiving pressure from surrounding cells, and that makes the cellular anode more stable and solid than the 2D one. Fig.5 shows the SEM images of cellular substrate after 63 cycles of Si anode. The cellular framework is kept stable even if it undertakes a huge internal stress, which is mainly attributed to the special stress distribution mentioned above.

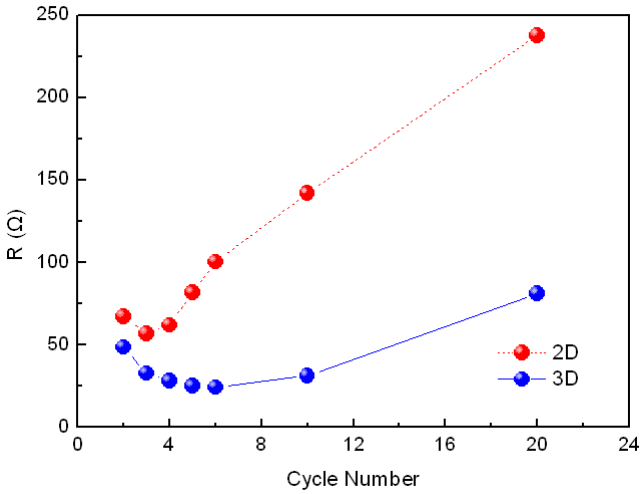

Figure 4. Resistance variation of cellular and 2D pure Si anodes as function of cycling, EIS measurements were conducted after the electrodes were charged up to 1.5V vs. Li/Li^+ at 0.01mA mg^{-1}.

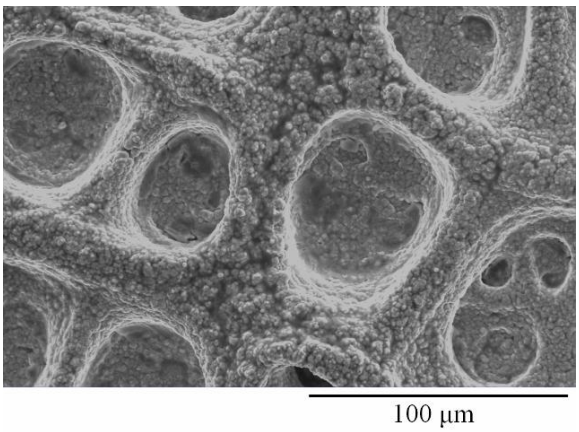

Figure 5. SEM micrograph of cellular substrate after 63 cycles of Si anode.

Despite the restriction of 3D framework, the active materials will not be restored to the original state before cycled just like an ideal elastic body. Therefore it must be pointed out that the stress-

induced failure in Si-based electrodes can be slowed down but not avoided by using of cellular substrate. Despite this problem, the cellular copper substrate has still shown great potential in ameliorating the cycling stability of new anode materials with high specific capacity.

4. CONCLUSIONS

Cellular Si-based anodes are prepared by casting milled Si and Si/C powders into the "valley-ridge" copper architecture. When selected discharging capacity is 800mAh/g, cellular pure Si electrodes have shown a better cycling performance than 2D ones and it can finish 63 cycles with a high coulombic efficiency. Moreover, the introduction of graphite can improve the cycling life of Si/C composite anodes to 152 cycles with an equivalent Li insertion depth to Si. The results of differential capacity plots and EIS measurements indicate that cellular substrate can provide a "stress- restriction" environment for active materials and suppress stain-induced loosening happened inside electrodes, which is helpful to improve the electrochemical performance.

ACKNOWLEDGEMENTS
This work was supported by the National Basic Research Program of China (973 Program) (2013CB934001), National Natural Science Foundation of China (51074011 and 51274017) and National 863 Program (2007AA03Z231 and 2011AA11A257).

References

1 P. Poizot, S. Laruelle, S. Grugeon, L. Dupont, J M. Tarascon, *Nature* 407 (2000) 496.
2 M. Winter, J. O. Besenhard, *Electrochim. Acta* 45 (1999) 31.
3 H. Li, Q. Wang, L. H. Shi, L. Q. Chen, X. J. Huang, *Chem. Mater*. 14 (2002) 103.
4 T. Takamura, S. Ohara, M. Uehara, J. Suzuki, K. Sekine, *J. Power Sources* 129 (2004) 96.
5 S. Ohara, J. Suzuki, K. Sekine, T. Takamura, *J. Power Sources* 136 (2004) 303.
6 H. Li, X. J. Huang, L. Q. Chen, Z. Wu, Y. Liang, *Electrochem. Solid-State Lett.* 2 (1999) 547.
7 H. C. Shin, J. A. Corno, J. L. Gole, M. L. Liu, *J. Power Sources* 139 (2005) 314.
8 G. X. Wang, J. H. Ahn, Jane Yao, Steve Bewlay, H. K. Liu, *Electrochem. Commun*. 6 (2004) 689.
9 H. Y. Lee, S. M. Lee, *Electrochem. Commun*. 6 (2004) 465.
10 N. Dimov, K. Fukuda, T. Umeno, S. Kugino, M. Yoshio, *J. Power Sources* 114 (2003) 88.
11 N. Dimov, S. Kugino, M. Yoshio, *J. Power Sources* 136 (2004) 108.
12 M. K. Datta, P. N. Kumta, *J. Power Sources* 158 (2006) 557.
13 C. Arbizzani, M. Lazzari, M. Mastragostino, *J. Electrochem. Soc*. 152 (2005) A289.
14 M. Yoshio, T. Tsumura, N. Dimov, *J. Power Sources* 146 (2005) 10.
15 M. S. Yazici, D. Krassowski, J. Prakash, *J. Power Sources* 141 (2005) 171.
16 T. Jiang, S. C. Zhang, X. P. Qiu, W. T. Zhu, L. Q. Chen, *J. Power Sources* 166 (2007) 503.
17 H. Li, X. J. Huang, L. Q. Chen, G. W. Zhou, Z. Zhang, D. P. Yu, Y. G. Mo, N. Pei, *Solid State Ionics* 135 (2000) 181.
18 M. N. Obrovac, L. Christensen, *Electrochem. Solid-State Lett*. 7 (2004) A93.
19 P. Limthongkul, Y. Jang, N. J. Dudney, Y. M. Chiang, *J. Power Sources* 119-121 (2003) 604.
20 M. Green, E. Fielder, B. Scrosati, M. Wachtler, J. S. Moreno, *Electrochem. Solid-State Lett*. 6 (2003) A75.

21 J. H. Ryu, J. W. Kim, Y. E. Sung, S. M. Oh, *Electrochem. Solid-State Lett*. 7 (2004) A306.
22 W. R. Liu, Z. Z. Guo, W. S. Young, D. T. Shieh, H. C. Wu, M. H. Yang, N. L. Wu, *J. Power Sources* 140 (2005) 139.
23 W. R. Liu, J. H. Wang, H. C. Wu, D. T. Shieh, M. H. Yang, N. L. Wu, *J. Electrochem. Soc*. 152 (2005) A1719.
24 Y. Zhang, X. G. Zhang, H. L. Zhang, Z. G. Zhao, F. Li, C. Liu, H. M. Cheng, *Electrochim. Acta* 51 (2006) 4994.
25 J. Y. Song, H. H. Lee, Y. Y. Wang, C. C. Wan, *J. Power Sources* 111 (2002) 255.
26 Y. C. Chang, H. J. Sohn, *J. Electrochem. Soc*. 147 (2000) 50.